Twelve port MIMO antenna with polarisation diversity for cognitive radio applications

D. Srikar✉ and S. Anuradha

In this letter, to overcome the drawbacks in reconfigurable antennas and maintain all the advantages in planar antennas, a compact 12 port integrated UWB and narrow band (NB)/wideband antennas for cognitive radio MIMO applications with polarisation diversity is presented. The proposed system has one pair of UWB antennas for sensing the spectrum and five pairs of NB/wideband antennas for communication. Each pair has two identical antennas, which are orthogonal to each other for polarisation diversity. Sensing antennas linked with ports (P1 and P7) have operating bandwidth of 3–11 GHz, whereas the antennas linked with ports (P2 and P8), (P3 and P9), (P4 and P10), (P5 and P11), and (P6 and P12) have operating bandwidths of 3.5–5.8 GHz, 2.8–3.5 GHz and 5.6–8 GHz (dual band), 8–8.4 GHz and 9–9.8 GHz (dual band), 8.4–9 GHz, and 9.8–11 GHz, respectively. Moreover, the overall volume of the antenna is 58mm × 50mm × 1.6 mm and the entire UWB spectrum is covered by NB/wideband antennas. Also, without any decoupling network, isolation of better than 20 and 15 dB is achieved between every two identical and non-identical antennas, respectively.

Introduction: In recent years, cognitive radio technology has witnessed a great demand, as it is a better solution to improve spectrum utilisation efficiency and mitigate spectrum overcrowdedness problem. Its operation is making the un-utilised spectrum available for other users when white spaces in the spectrum are identified. MIMO systems have been the most promising systems to overcome multipath fading problems. Moreover, MIMO antennas with polarisation diversity enhance the channel capacity in both line-of-sight and non-line-of-sight (NLOS) propagations. In [1], a sensing antenna was incorporated between two reconfigurable MIMO antennas. Depending on the statuses of PIN diodes, reconfiguration in the frequency bands 3.2–4.0 GHz and 4.8–6.2 GHz was achieved in MIMO elements. However, entire UWB was not covered. In [2], a four port antenna which consists of two sensing antennas and two reconfigurable filtennas in interweave scenario was presented. Reconfiguration was achieved by incorporating PIN diodes as switches in the feed lines of filtennas. Conventionally, single port reconfigurable UWB/narrow band (NB) antenna and dual-port-integrated UWB and reconfigurable NB antennas [3–5] are mostly used for cognitive radio applications. However, when multiple spectrum holes are identified, systems with integrated UWB sensing antenna and multiple wideband/NB antennas are highly preferred to improve spectrum utilisation efficiency. However, the main challenges present in this design are isolation and space limitation. More importantly, the drawbacks associated with reconfigurable antennas [3] can be overcome and all the advantages of the planar antennas can be captured. However, here also, the excitation switching reconfigurable mechanism is done among all the wideband/NB antennas based on the unused spectrum holes identified.

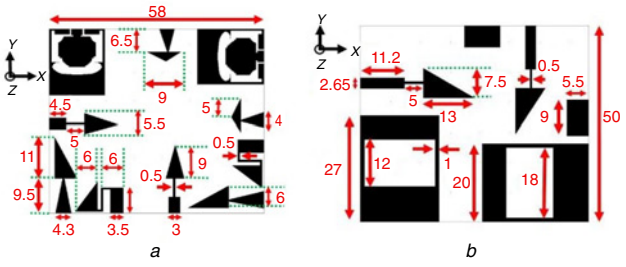

Fig. 1 *The proposed antenna (all dimensions are in mm)*

a Top view
b Bottom view

In this letter, a 12 port MIMO antenna with polarisation diversity for cognitive radio platforms is reported. Among the 12 antennas, two similar UWB antennas are dedicated for sensing purpose and the remaining ten wideband/NB antennas are used for communication. Polarisation diversity and high isolation between the similar antennas are achieved by placing each pair of similar antennas perpendicular to each other. The overall area of the proposed MIMO antenna is 58×50 mm^2. To our knowledge, no MIMO antenna with polarisation diversity for cognitive radio platforms with multiple wideband/NB antennas used for communication purpose has been presented so far. The configuration of the proposed antenna, top and bottom views of the fabricated prototype are depicted in Figs. 1, 2*c*, and *d*, respectively. Also, the fabricated antenna is tested by using Agilent N5232A PNA-L network analyser to demonstrate its functionality. The simulated and measured s-parameters of all the antennas in the 12 port MIMO system are shown in Figs. 3–5.

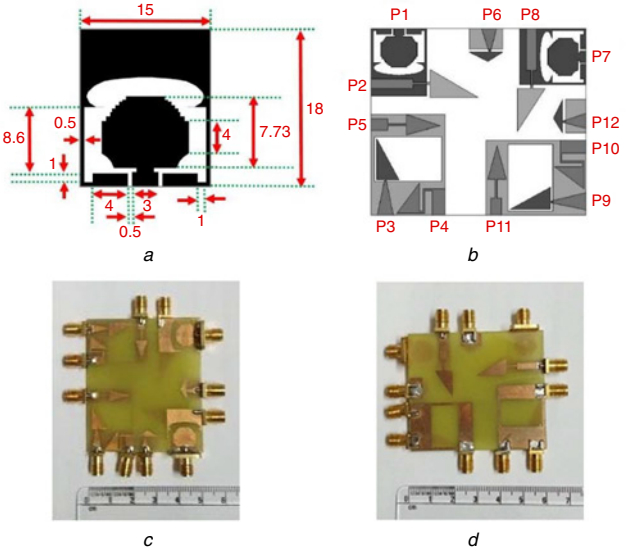

Fig. 2 *Configurations of the sensing, proposed 12 port MIMO antennas and photographs of the fabricated prototype*

a Geometry of the UWB sensing antenna (dimensions in mm)
b Final structure of the antenna
c Top view of the proposed antenna's prototype
d Bottom view of the proposed antenna's prototype

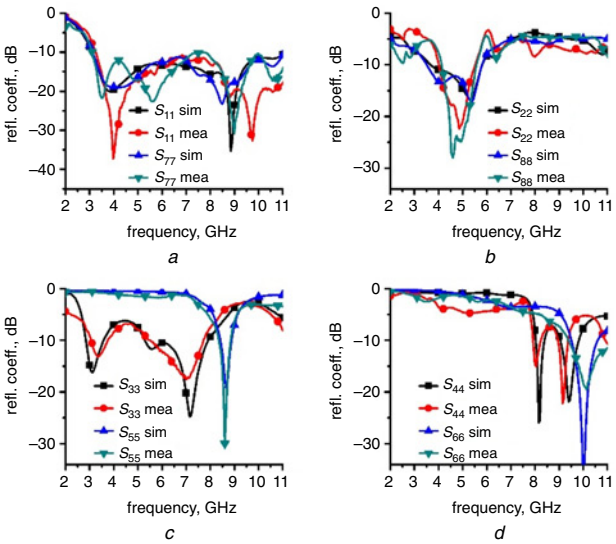

Fig. 3 *Input reflection coefficients of ports 1, 2, 3, 4, 5, 6, 7, and 8*

a Plot of S_{11} and S_{77}
b Plot of S_{22} and S_{88}
c Plot of S_{33} and S_{55}
d Plot of S_{44} and S_{66}

Antenna design: The design process starts with the design of UWB antenna. Initially, a compact UWB antenna of area 15×18 mm^2 is designed, as shown in Fig. 2*a*. By properly choosing the dimensions of widths of the wide rectangular slot, two rectangular notches, and 'Ω' shaped notch in the ground plane, impedance matching at the lower frequencies is achieved. Later, the rectangular patch is modified to achieve impedance matching at the mid frequencies of UWB and the modified patch is fed by a microstrip line of impedance >50 Ω

added with a strip line of impedance 50 Ω for impedance matching purpose at higher frequencies of the UWB. The reflection coefficient performance of UWB sensing antenna linked with port 1 is shown in Fig. 3*a*. Thereafter, as illustrated in Fig. 2*b*, beneath the ground plane of the UWB antenna, a very thin strip line of 0.5 mm width is used in between right-angled triangular-shaped radiator and 50 Ω strip line to produce a wideband ranging from 3.5 to 5.8 GHz which is shown in Fig. 3*b*. The length of 0.5 mm strip line controls the resonance at the lower frequencies of the band. Despite the antenna linked with port 2 shares common ground with UWB sensing antenna, isolation of better than 13 dB is achieved in the entire UWB, as depicted in Fig. 5*b*. This is due to the fact that current flow directions at all frequencies in the UWB sensing antenna and antenna linked with port 2 are orthogonal to each other. Moreover, the other reason is due to the weak surface currents at the ground plane exactly above feed line of antenna linked with port 2 at all the frequencies in UWB when sensing antenna is excited, as depicted in Fig. 6. As illustrated in Fig. 3*c*, the antenna linked with port 3 is a dual-band antenna, which covers communication bands, i.e. 2.8–3.5 GHz and 5.6–8 GHz due to two distinct current paths. From the surface current distribution plots, it is evident that the resonance at the lower frequencies of Antenna linked with port 3 is due to the longer electrical length provided by the extended ground plane, as shown in Fig. 6. Whereas the active right-angled triangular patch is responsible for the resonance at higher frequencies, as shown in Fig. 6.

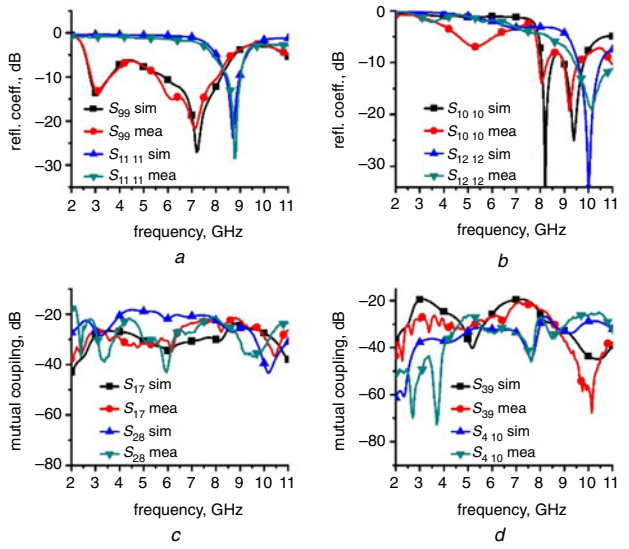

Fig. 4 *Input reflection coefficients of ports 9, 10, 11, and 12 and mutual coupling between ports 1 and 7, 2 and 8, 3 and 9, and 4 and 10*

a Plot of S_{99} and $S_{11\,11}$
b Plot of $S_{10\,10}$ and $S_{12\,12}$
c Plot of S_{17} and S_{28}
d Plot of S_{39} and $S_{4\,10}$

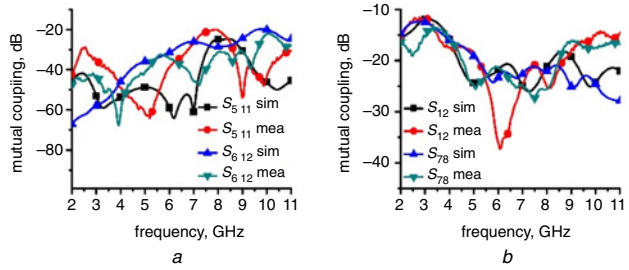

Fig. 5 *Mutual coupling between ports 1 and 2, 7 and 8, 5 and 11, and 6 and 12*

a Plot of $S_{5\,11}$ and $S_{6\,12}$
b Plot of S_{12} and S_{78}

Antenna linked with port 4 covers two communication bands i.e. 8–8.4 GHz and 9–9.8 GHz, as shown in Fig. 3*d*. To achieve impedance matching in these bands, a meander line type feed structure is used, as depicted in Fig. 2*b*. Antenna linked with port 5 is a NB antenna, which has an operating bandwidth of 8.4–9 GHz, as shown in Fig. 3*c*. Impedance matching is achieved by selecting the proper length of the 0.5 mm strip line, which is in between the triangular patch and 50 Ω feed line, as shown in Fig. 2*b*. Although the antennas linked with ports 3, 4, and 5 share common ground, minimum isolation of better than 15 dB in the entire UWB is achieved among these antennas. Their current flow directions and placements ensure good isolation among them which can be understood from the surface current distribution plots shown in Figs. 6 and 7.

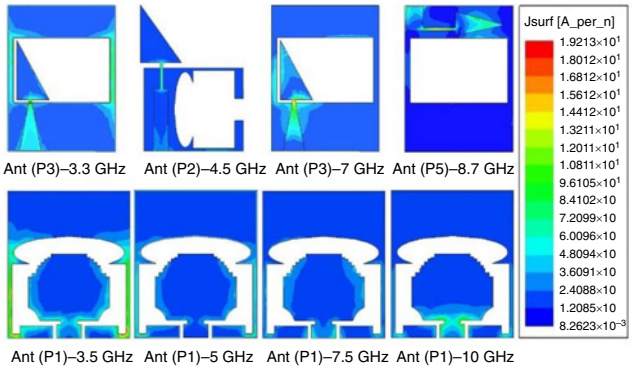

Fig. 6 *Surface current distributions of the antennas linked with port 3 at 3.3 and 7 GHz, port 2 at 4.5 GHz, port 5 at 8.7 GHz, and port 1 at 3.5, 5, 7.5 and 10 GHz*

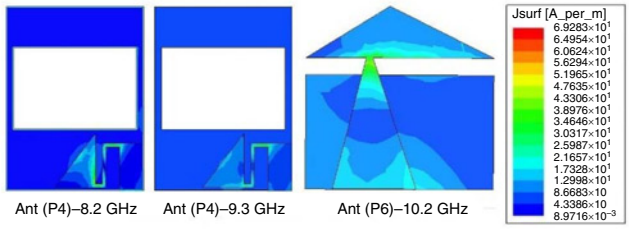

Fig. 7 *Surface current distributions of the antennas linked with port 4 at 8.2 and 9.3 GHz and port 6 at 10.2 GHz*

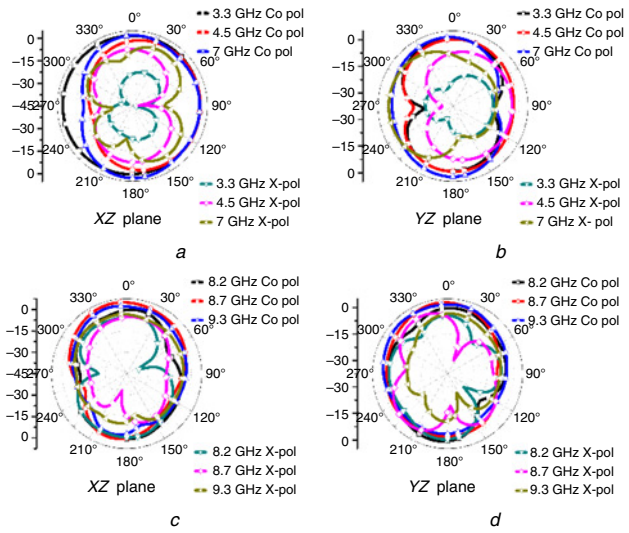

Fig. 8 *Measured radiation patterns of the antennas linked with*

a Port 2 at 4.5 GHz and port 3 at 3.3 and 7 GHz in *XZ* plane
b Port 2 at 4.5 GHz and port 3 at 3.3 and 7 GHz in *YZ* plane
c Port 4 at 8.2 and 9.3 GHz and port 5 at 8.7 GHz in *XZ* plane
d Port 4 at 8.2 and 9.3 GHz and port 5 at 8.7 GHz in *YZ* plane

For the sake of brevity, isolation plots among the antennas linked with ports 3, 4 and 5 are not presented. Antenna linked with port 6 is an asymmetrically fed monopole antenna with a tapered feed line, which has an impedance bandwidth of 9.8–11 GHz, as shown in Fig. 2*i*. Whenever a spectrum hole is identified, the NB/wideband antenna, which operates in that spectrum, is used for communication purpose. Meanwhile, the remaining antennas used for communication are terminated with 50 Ω load.

For MIMO antenna system with polarisation diversity, the identical antennas are placed in such a way that their current flow directions are orthogonal to each other. Moreover, due to their placement, without using any isolation technique, good isolation levels of better than 20 dB are achieved, as illustrated in Figs. 4 and 5*a*.

Results and discussion: The measured radiation patterns of the antennas coupled with ports 1, 2, 3, 4, 5 and 6 in orthogonal planes are shown in Figs. 8 and 9. During measurement time, only one port is excited and the rest of the ports are terminated with 50 Ω load. At 4.5 GHz, the antenna linked with port 2 has maximum gains of 0.2 and 0.6 dBi in end fire direction in *XZ* and *YZ* planes, respectively, as shown in Figs. 8*a* and *b*. Since the antenna linked with port 2 is asymmetrically fed monopole antenna, the existence of horizontal surface currents causes maximum cross pol levels to reach −7.3 and −4 dB in *XZ* and *YZ* planes, respectively. As illustrated in Figs. 8*a* and *b*, at 3.3 GHz, the antenna linked with port 3 has monopole like radiation patterns in both the planes, whereas nearly omnidirectional patterns are observed in both the planes at 7 GHz.

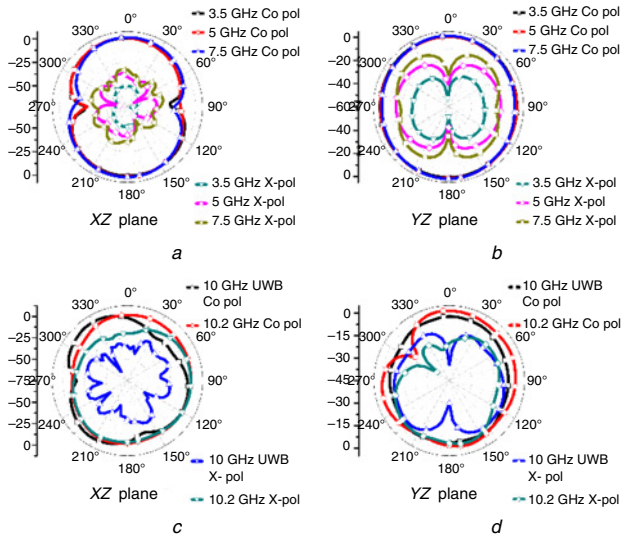

Fig. 9 *Measured radiation patterns of the antennas linked with*

a Port 1 at 3.5, 5 and 7.5 GHz in *XZ* plane
b Port 1 at 3.5, 5, and 7.5 GHz in *YZ* plane
c Port 1 at 10 GHz and port 6 at 10.2 GHz in *XZ* plane
d Port 1 at 10 GHz and port 6 at 10.2 GHz in *YZ* plane

As depicted in Figs. 8*a* and *b*, there is a significant rise of cross pol at 7 GHz in both the planes due to its asymmetrically fed monopole like structure of the antenna. However, in indoor wireless communication systems, where channels are influenced by Rayleigh fading, cross pol performance is not a vital requirement. The antenna linked with port 4 has patterns which are partly bidirectional and directional in nature in both the planes at 8.2 and 9.3 GHz, respectively, as shown in Figs. 8*c* and *d*.

Due to its defected ground structure, the antenna linked with port 5 has the directional pattern with a little back radiation in *XZ* plane, whereas it has a nearly omnidirectional pattern in *YZ* plane at 8.7 GHz, as shown in Figs. 8*c* and *d*. At 10.2 GHz, the antenna linked with port 6 has nearly omnidirectional patterns in the orthogonal planes, as shown in Figs. 9*c* and *d*. From Figs. 9*a* and *b*, it can be seen that in case of UWB sensing antenna linked with port 1, at three sampling frequencies (3.5, 5, and 7.5 GHz), dumbbell-shaped patterns in *XZ* plane and omnidirectional patterns in *YZ* plane are achieved. As illustrated in Figs. 9*c* and *d*, at higher sampling frequency 10 GHz, nearly omnidirectional patterns in both the planes are achieved and cross polarisation significantly grows due to the horizontal current modes.

The measured peak gains and radiation efficiencies of the UWB sensing antenna and the antennas used for communication purpose are shown in Figs. 10*a* and *b*, respectively. In order to evaluate the diversity performance of the proposed MIMO antenna, the parameters like envelope correlation coefficient (ECC) and diversity gain (DG) are calculated using [4]. From Figs. 10*c* and *d*, it is observed that measured DG between any two identical antennas used for the purpose of communication is ∼10 dB and ECC between any two identical antennas used for communication is <0.004, which specifies the good diversity performance of the proposed MIMO antenna.

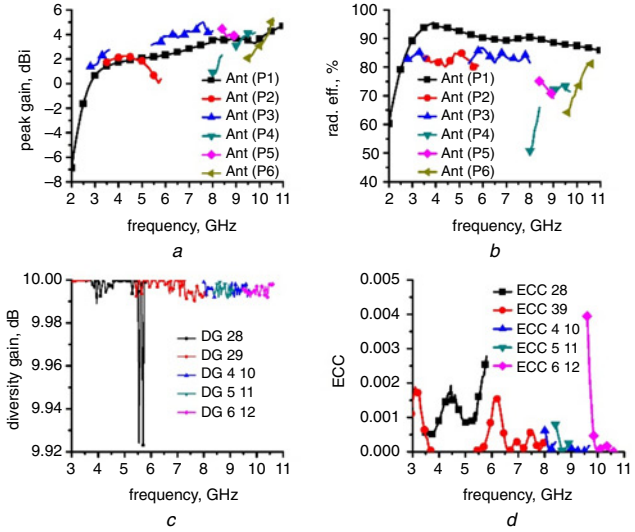

Fig. 10 *Measured peak gains, radiation efficiencies, ECC, and DG of the proposed MIMO antenna*

a Peak gains of the antennas for sensing and communication
b Radiation efficiencies of the antennas for sensing and communication
c DG of every two identical antennas used for communication
d ECC of every two identical antennas used for communication

Conclusion: A 12 port MIMO antenna with polarisation diversity for cognitive radio applications has been presented. The five pairs of antennas used for communication have single bands and dual bands to cover the entire spectrum of UWB and the two UWB antennas used for sensing purpose cover total spectrum of UWB. Polarisation diversity is achieved by placing every identical pair of antennas orthogonal to each other. Isolation of better than 20 dB is achieved between every two identical antennas. The consistency of the proposed MIMO antenna has been shown by comparing the simulated and measured results. ECC and DG have been calculated to characterise diversity performance. The proposed antenna system enhances the spectrum utilisation efficiency by providing multiple communications when multiple spectrum holes are detected. Since the proposed MIMO antenna has five pairs of antennas for communication purpose, it can perform a maximum of five communication tasks simultaneously. Moreover, the proposed antenna is very compact, simple, and inexpensive.

Submitted: *13 July 2019* E-first: *12 September 2019*
doi: 10.1049/el.2019.2291
One or more of the Figures in this Letter are available in colour online.

D. Srikar and S. Anuradha (*Department of Electronics and Communications Engineering, National Institute of Technology Warangal, Warangal 506004, Telangana, India*)

✉ E-mail: srikard86@gmail.com

References

1 Srivastava, G., Mohan, A., and Chakrabarty, A.: 'Reconfigurable MIMO slot antenna with UWB sensing capability'. Asia Pacific Microwave Conf., Kuala Lumpar, Malaysia, November 2017, pp. 184–187
2 Tawk, Y., Costantine, J., and Christodoulou, C.G.: 'Reconfigurable filtennas and MIMO in cognitive radio applications', *Trans. Antennas Propag.*, 2014, **62**, (3), pp. 1074–1083
3 Nella, A., and Gandhi, A.S.: 'A survey on planar antenna designs for cognitive radio applications', *Wirel. Person. Commun.*, 2018, **98**, (1), pp. 541–569
4 Pahadsingh, S., and Sahu, S.: 'Four port MIMO integrated antenna system with DRA for cognitive radio platforms', *Int. J. Electron. Commun. AEU.*, 2018, **92**, pp. 98–110
5 Hussain, R., and Sharawi, M.S.: 'A cognitive radio reconfigurable MIMO and sensing antenna system', *Antenna Wirel. Propag. Lett.*, 2015, **14**, (1), pp. 257–260